

**NASA  
Technical  
Paper  
2789**

February 1988

**Dynamic Analysis  
of Multimesh-Gear  
Helicopter Transmissions**

Fred K. Choy,  
Dennis P. Townsend,  
and Fred B. Oswald

(NASA-TP-2789) DYNAMIC ANALYSIS OF  
MULTIMESH-GEAR HELICOPTER TRANSMISSIONS  
(NASA) 22 P CSDL 131

N88-17045

H1/37 Unclas  
0124535

**NASA**

**NASA  
Technical  
Paper  
2789**

1988

# Dynamic Analysis of Multimesh-Gear Helicopter Transmissions

Fred K. Choy,  
Dennis P. Townsend,  
and Fred B. Oswald

*Lewis Research Center  
Cleveland, Ohio*



National Aeronautics  
and Space Administration

Scientific and Technical  
Information Division

## Summary

A dynamic analysis of multimesh-gear helicopter transmission systems was performed by correlating analytical simulations with experimental investigations. Two computer programs were used in this study, GRDYNMLT and PGT, both of which were developed under NASA/Army sponsorship. Parametric studies of the numerical model with variations in mesh damping ratios, operating speeds, tip-relief tooth modifications, and tooth-spacing errors were performed to investigate the accuracy, application, and limitations of the two computer programs. Results from analytical work were compared with experimental data obtained from the U.S. Army's UH-60A Black Hawk 2240-kW (3000-hp) class, twin-engine helicopter transmission tested at the NASA Lewis Research Center.

The investigation revealed that both computer programs predicted similar levels of gear dynamic loading under identical operating conditions. Program GRDYNMLT was found to be more versatile in application and in modeling complexities, such as large number of planets, varieties of configuration, helical gear system, and tooth-profile modification. In addition, GRDYNMLT also provided other dynamic characteristics, such as stresses, temperature, pressure-velocity factor, and Hertz stresses, that are vital to gear design. Results from the parametric study using GRDYNMLT showed that gear system dynamics can vary significantly with changes in gear mesh damping. By correlating the analytical simulation from GRDYNMLT with experimental data, a more realistic value for mesh damping can be obtained.

## Introduction

A considerable amount of noise is generated by gear teeth as they transmit loads at operating speeds. This noise is the result of dynamic tooth loads transmitting vibration to the shafts and structural elements of the transmission system. Several methods have been tried in attempting to reduce or eliminate the dynamic load and thus the gear noise. Reference 1 shows that the noise level of a gear mesh can be reduced by about 5 dB through profile modification (tip relief). Increasing the contact ratio to 2 or 3 should reduce the dynamic

tooth load by keeping the gear tooth spring constant more uniform (ref. 2), thus allowing a more uniform load transmission between gear teeth.

Several years ago, the effects of high contact ratio and tooth-profile modification were investigated to determine their effects on gear tooth dynamic loads. The investigation included both an experimental and an analytical evaluation of gear dynamic loads for standard and high-contact-ratio gears (i.e.,  $>2$ , refs. 3 and 4). The initial analytical results were used to design test gears for experimental testing. It was then found that design analysis based on constant tooth-mesh stiffness did not give the best design and that, in fact, the fabricated gears experienced tooth-bending failures. The analytical program was modified to include the effects of variable tooth stiffness and various methods of tooth-profile modification. The improved analysis gave much better correlation with experimental results.

This initial analytical computer code was developed for a single-mesh dynamic analysis. Because most helicopter transmissions utilize a planetary gear system, the program was expanded to include multiple-mesh gear dynamic analysis that would determine the dynamic loads in the sun-planet and ring-planet meshes of a planetary gear system with several planets.

Over a period of time, two computer programs were developed to determine dynamic loads for planetary gears. The original NASA/Army-sponsored single-mesh computer code, GRDYNMESH, was developed into a multimesh computer program for planetary gears (refs. 5 and 6). Another NASA/Army grant also developed a computer program, PGT, for dynamic analysis of planetary gears, this time using a different approach for analyzing the system dynamic load and frequencies (ref. 7).

The objective of the present study was to perform parametric studies of two planetary transmissions by using the two different analytical programs and then comparing the analytical results with each other and with experimental results from tests on the U.S. Army's Black Hawk helicopter. In addition, each program was evaluated for capabilities, limitations, and accuracy in predicting tooth loads, frequencies, and stresses. The results of this study are presented in three major categories: analytical simulation, parametric study and experimental correlation, and comparison of the two programs.

# Transmissions and Analysis Methods

## Test Planetary Transmissions

Two multimesh planetary gear transmission systems were used in this particular study: the UH-60A 2240-kW (3000-hp) Black Hawk helicopter transmission, and the NASA/Bell Helicopter experimental 370-kW (500-hp) helicopter transmission system. A schematic of the UH-60A transmission system is shown in figure 1, and the basic design data are given in table I. The system consists of two input modules and one main module, with a total speed reduction of 81.042. The main module consists of a 62-tooth sun gear that drives five 83-tooth planetary gears, with the carrier splined to the output rotor shaft. The stationary ring gear has 228 teeth. With the input speed of the sun gear at 1207 rpm, the carrier output speed is reduced to 258 rpm. A more detailed description of the Black Hawk transmission system is given in references 8 and 9. The other system used in this analysis is the NASA 370-kW (500-hp) high-contact-ratio planetary transmission. It consists of a 27-tooth sun gear, four 35-tooth planetary gears, the planet carrier, and a stationary 99-tooth ring gear. A schematic of the system is given in figure 2. The sun-planet mesh and ring-planet mesh are of nonstandard center distances (nonstandard involute proportions). A more detailed description of the system is given in reference 10.

## Computer Codes

Two computer codes were used in this study: GRDYNMLT, developed under a NASA/Army contract (refs. 5 and 6), and PGT (ref. 7), developed under a NASA/Army research grant. GRDYNMLT is a multimesh-gear analysis code that runs on the IBM-370 system; PGT is a three-planet-gear mesh analysis code that runs on the HP-1000 minicomputer system. Two additional auxiliary computer codes were used in this study. They are GRDYNSNG (refs. 3 and 4), a single-mesh analysis code that runs on the Cray II, and FREPL (ref. 11), a frequency-domain analysis code developed at NASA Lewis that runs on the IBM-370.

The program GRDYNMLT was developed to handle various types of multimesh epicyclic gear systems with external, internal, buttress-spur, or helical tooth forms. It can handle up to 20 planets with spur or helical gear configurations. The

TABLE I.—BASIC DESIGN DATA FOR UH-60A 2240-kW (3000-hp) HELICOPTER TRANSMISSION

[Number of planets, 5.]

	Sun	Planet	Planet	Ring
Number of teeth	62	83	83	228
Diametral pitch	8.857	8.857	8.857	8.857
Pressure angle, deg	22.5	22.5	22.5	22.5
Face width, cm (in.)	8.15 (3.21)	7.58 (2.965)	7.53 (2.965)	6.05 (2.38)
Speed, rpm	1207	450.7	450.7	0

program analysis includes effects such as variable contact friction, planet-gear and ring-gear rim support flexibilities, tooth-profile modification with tip relief, and tooth-spacing error. A numerical iteration scheme is applied in the program to solve the dynamic equations of motion with the assumed boundary conditions. Results of this analysis are presented in three phases: (1) dynamic characteristics of each gear mesh including dynamic load, stress, and flash temperature along the line of action, (2) dynamic gear load for 10 single-tooth passes after a tooth geometric error, and (3) maximum mesh load with an operating speed increment. The results of the 10 tooth passes were also used by program FREPL for frequency-domain analysis.

The program PGT was developed by using numerical integration techniques to generate a steady-state solution for the gear-mesh system from initial transient conditions. The program can handle only spur-gear mesh with the ring gear being stationary and can analyze only a three-planet system. Mesh load and gear stiffness are calculated for each sun-planet and ring-planet mesh. The motion of the floating sun gear is generated.

## Results and Discussion

The results of this study are presented in three major categories: (1) various analytical simulations and their applications in gear design, (2) parametric studies of various mesh damping ratios and the effects of tooth modifications and their correlations with experimental data, and (3) comparison of the analytical results and limitations of the two computer programs GRDYNMLT and PGT. Each of these major categories will be examined through the three analytical phases discussed earlier.

### Analytical Simulations

The UH-60A Black Hawk 2240-kW (3000-hp) helicopter gear transmission system was used to illustrate the various analytical simulations in this study. Three phases of analytical simulations were performed to achieve maximum evaluation of the system. The first phase was a dynamic analysis of the system at operating speed with no tooth error. Figures 3(a) to (e) show the results of the first sun-planet mesh dynamics during a single-tooth-pass cycle. Similar results were also obtained for the ring-planet mesh and other gear meshes. Figure 3(a) shows the dynamic mesh load at various stages of engagement and disengagement during a single-tooth pass. The overlapping of the solid and dashed lines indicates that more than one tooth was participating in the mesh interaction (contact ratio greater than 1.0) during the single-tooth pass. (The distances along the line of action are normalized in the figure and are discussed in more detail in appendix A.) Figure 3(b) represents the pressure-velocity values during the tooth pass, which can be used to estimate scoring (ref. 12). Figures 3(c) and (d) show the Hertz stress and flash

temperature of the gear tooth during the tooth pass and will provide information for pitting fatigue calculation (ref. 13). Figures 3(e) and (f) are the maximum bending stresses for both the sun-gear tooth and planet-gear tooth during meshing, which are useful for both design and high- or low-cycle fatigue analysis.

The second phase of this analysis included the effects of tooth-spacing errors. In addition to the results presented in the first phase, the analysis also simulated the system dynamics for the next 10 single-tooth passes. This ensured a more comprehensive representation of the dynamic behavior of the system with the noninteger type of gear ratio. Figure 4(a) shows the tooth loads for the 10 single-tooth-pass cycles in the time domain. Using the Cooley-Tukey fast Fourier transform approach (ref. 14) produced the frequency-domain data for the mesh load given in figure 4(b). Note that in addition to the average mesh load (indicated at zero frequency for use in fatigue or fracture analyses), the frequency data also provide the magnitudes of excitation at various dominating frequency components.

The third phase was the multispeed analysis. Figure 5 shows the maximum load of the first mesh over an operating speed range. This analysis not only provided designers with valuable information on the dynamics of the system during startup or coastdown operations, but also indicated the natural frequency components at various operating speeds. A more detailed discussion of the natural frequency prediction and experimental results correlation is presented in the next section.

An attempt was made to analyze the NASA/Bell Helicopter experimental 370-kW (500-hp) helicopter transmission system. Because of the nonstandard gear configuration between both the sun-planet and ring-planet meshes, no convergence in solution could be achieved by the dynamic equations, assuming standard gear meshes. The single-mesh option of GRDYNMLT was then used with each individual sun-planet and ring-planet mesh separately. The mesh data were assembled and used as input to the multimesh program GRDYNMLT. This attempt also was unsuccessful because the organization in GRDYNMLT was such that some of the stiffnesses generated within the program itself were not consistent with the input of a nonstandard mesh assembly. It was concluded that a nonstandard gear system is beyond the capabilities of GRDYNMLT until major revisions are made in the program.

## Parametric Studies

A parametric study of the effects of mesh damping ratios on the UH-60A Black Hawk 2240-kW (3000-hp) transmission was performed to correlate the analytical simulations more consistently with the experimental results and to achieve a better understanding of the system dynamic behavior. The first phase of this parametric study determined the dynamic characteristics of the gear during one single-tooth pass. Figures 6 to 8 present the dynamic tooth load, the Hertz stress, and the maximum bending stress, respectively, of the first sun-planet mesh along the line of action for a range of mesh damping

ratios from 0.02 to 0.2. The dynamic tooth load, Hertz stress, and maximum bending stress all behaved similarly with the change in mesh damping ratio. At a damping ratio of 0.02, four dominant peaks were produced during one single-tooth pass. As the damping ratio was increased, the peaks became less pronounced and were almost undetectable at high damping. The existence of the fourth-order, tooth-pass frequency harmonic is due to the nonsynchronous meshing of the other planets. The phasing constants for various planets of the UH-60A system are given in table II. (The calculation of the phasing constants is described in appendix B.) With light damping (fig. 6), the maximum loads for the sun-planet mesh occurred at normalized distances along the line of action that were close to the phasing constants. These maximum-load locations shifted considerably as damping was increased. The dynamic loading on the ring-planet mesh is given in figure 9. Figure 10 gives the maximum bending stress for a ring-gear tooth during one single-tooth pass and also shows dynamic characteristics similar to those for the sun gear. With large damping, a more pronounced phase delay resulted from the ring-planet mesh load (fig. 10) than from the sun-planet mesh load (fig. 8). The reason is that when the sun gear is the driver, more direct action is imposed onto the sun-planet mesh than onto the ring-planet mesh.

In the second phase of the parametric study, the four-times-per-single-tooth-pass frequency was further confirmed by using fast Fourier transform techniques to examine the frequency components. Figure 11 depicts the mesh load for various damping ratios during 10 consecutive single-tooth passes with tooth-spacing error. The overlapping of the curves shows each tooth-load participation in the mesh. The peak loads were much higher at low damping, as would be expected in any mechanical system. Comparing figures 11 and 12 shows that for the lightly damped system the peak load in the time domain was higher than for the higher damping ratios but the average load in the frequency domain was slightly lower. This was due to the considerably larger load variation experienced in the lightly damped system, which resulted in a slightly lower sum over the tooth-pass period. Since the total transmitted load for the overall global gear system remained constant, other meshes would have to share a higher average load in order to compensate for such a loss. Also, the fourth-order, tooth-pass

TABLE II.—PLANET-MESH PHASING CONSTANTS<sup>a</sup>

Mesh	Sun-planet (eq. (1))	Ring-planet (eq. (2))
First	0	0
Second	.4	.6
Third	.8	.2
Fourth	.2	.8
Fifth	.6	.4

<sup>a</sup>See appendix B for calculation of phasing constants.

component (3900 Hz) was more pronounced at lower damping, as predicted by the tooth-load stress analysis in figures 6 to 8.

Figure 13 gives the dynamic tooth load for the other four meshes with tooth-spacing error at a low damping ratio (0.02). As a result of phasing, the dynamic tooth load varied considerably among the meshes. The load vanished several times in one single-tooth pass for the second mesh, indicating that several engagement-disengagement cycles occurred during a single-tooth pass. During such an engagement-disengagement process, the maximum dynamic tooth load is greatly increased, thereby significantly increasing the vibration and noise of the entire system. Figure 14 depicts the frequency components of each mesh load. The second mesh, which experienced several total disengagements during one single-tooth pass, had the highest fourth-order, tooth-pass frequency component. This indicated that a more dominating fourth harmonic of the tooth-pass frequency could be expected. With the exception of the fifth mesh, the average mesh loads remained nearly constant. The fifth mesh was lightly loaded as a result of phasing and tooth-spacing error.

The analytical results showing the effects of tooth-profile modifications at the first mesh are presented in figure 15. Note that the total dynamic load for the mesh remained constant. The use of tooth-profile modification reduced the peak tooth-load magnitude at engagement-disengagement but increased the peak load due to phasing. This load increase can result in higher tooth stress as well as further amplify the multiple harmonic of the tooth-pass frequency. Although gear noise can be reduced by tooth-profile modification (refs. 1 and 2), the resulting increase in stress level may not be desirable.

In order to verify the analytical simulations, results from the first and second phases of the parametric study were compared with experimental data obtained from the NASA Lewis gear testing facility. Ring-gear stresses were monitored at both the fillet and the root, but sun-gear stresses only at the root. A section of the ring-gear fillet gage data for 10 planet passes is given in figure 16(a). Figures 16(b) and (c) present, respectively, the ring-gear fillet and root stresses for a single-planet pass in a zoom-in format. In these figures, the maximum fillet and root stresses are of the same order of magnitude. A similar conclusion was reached by Drago (ref. 15) for thin-rim gear systems under high loading. For these reasons (and in the absence of experimental sun-gear fillet stresses), the sun-gear root stresses were used in this correlation. Figure 16(d) presents a comparison of the analytically calculated bending stress with the experimental fillet stress data for the ring gear. Good correlations are evident in the peak magnitude of the ring stresses for an assumed mesh damping ratio of 0.02. In order to explore the vanishing of the multiple harmonics in the experimental data, as well as to better correlate the results,

the sun- and ring-gear stresses were examined in more detail.

Figure 17 shows the sun- and ring-gear root stress averaged over 10 tooth-pass interactions with a filter cutoff frequency of 1800 Hz. The maximum compressive root stress for the sun gear was 510 MPa (74 ksi), and the maximum tensile root stress for the ring gear was 496 MPa (72 ksi). The analytical simulations (fig. 8) predicted maximum sun-gear fillet stresses of 496 MPa (72 ksi) at 0.02 and 296 MPa (43 ksi) at 0.2. According to Drago (ref. 15), under large bending stress at the gear tooth, the maximum root compressive stresses and fillet tensile stresses should have similar orders of magnitude (ref. 15). The sun-gear root stresses were measured at the center of the root. Figure 10 shows that the ring-gear fillet tensile stress can vary from 448 MPa (65 ksi) at a mesh damping ratio of 0.02 to 310 MPa (45 ksi) at 0.2. The experimental data and the analytical results indicated that a sun-planet mesh provides less damping because of the floating sun arrangement. This is in accord with previous results. A closer examination of the experimental data confirmed this indication.

Figure 18(a) shows the unfiltered (anti-aliasing filter set at 20 kHz) and unaveraged strain gage data for the ring-gear fillet stress during a tooth-pass interaction. The zoom-in data in figure 18(b) reveal that some peak values of the maximum bending stress still existed during the single-tooth pass. The lack of distinction in the peak amplitudes and their lower numbers are probably due to material damping, which was not modeled in the analytical simulation.

In order to correlate experimental data with the third phase (peak amplitude speed analysis) of the analytical simulation, a waterfall diagram of the gearbox accelerometer vibration data at various carrier speeds was made (fig. 19). At full speed (267 rpm), the first four harmonics of the tooth mesh can be detected as predicted in the second phase of this study. Three major natural frequencies occurred at carrier speeds of 100, 180, and 220 rpm (corresponding to sun-gear speeds of 450, 810, and 990 rpm). The maximum tooth loads predicted by the analytical simulations at various sun-gear speeds (fig. 20) occurred at approximately 420, 700, and 900 rpm. Correlating the natural frequencies in figures 19 and 20 confirmed the validity of the analytical model. The difference between the analytical work and the experimental data in regard to the ratio of magnitudes among various peaks was primarily due to the various damping effects of the bearing supports and the gearbox structure that were modeled in the analytical simulations. The frequencies appearing in the accelerometer data, but not predicted by the analytical simulation, resulted from other component inputs not in the numerical model. Overall, the major dynamic behavior was predicted closely by the computer simulation.

### Comparisons Between Computer Programs GRDYNMLT and PGT

In order to obtain a comparison between the two computer codes, a three-planet gear transmission model was set up. Because of the limitations in the computer programs, only dynamic tooth loads were compared rather than the three-phase study presented in the previous section. Figure 21 depicts the gear-mesh loads predicted by the PGT program at both the sun-planet and ring-planet meshes. The highest loads predicted were approximately 5660 N (1250 lb) for the first sun-planet mesh and 3335 N (750 lb) for the first ring-planet mesh. Figure 22 shows the gear-mesh load for both the first sun-planet and the first ring-planet meshes for each tooth as predicted by the program GRDYNMLT. The total maximum loads were predicted to be 4900 N (1100 lb) for the first sun-planet mesh and 3560 N (800 lb) for the first ring-planet mesh. The two programs seemed to predict a similar level of gear-mesh load. A plot of the orbit of the floating sun gear is given in figure 23. The three outside lobes show that a dominating two-times-synchronous component exists in the system. This can also be seen in the mesh load in figure 21. Since gear-mesh load and sun-gear movement are the only major outputs from the PGT program, comparing other results was impossible. The major analytical results of the two programs are compared in table III, with comments on their features being given in table IV. The results show program GRDYNMLT to be superior to PGT in many respects.

TABLE III.—COMPARISON OF PROGRAMS

Characteristic	Program	
	GRDYNMLT	PGT
Maximum number of planets	20	3
Helical gearing?	Yes	No
Rotating ring?	↓	No
Floating sun?	↓	Yes
Profile modification?	↓	No
Multispeed analysis?	↓	↓
Variable contact friction?	↓	↓
Nonstandard gear?	No	↓
Tooth-spacing error?	Yes	Yes
High contact ratio (>2)?	Yes	No
Convergence	Usually good	Did not converge with large torque
Sun orbit	Not provided	Provided

TABLE IV.—FEATURES OF PROGRAMS

Feature	Operating system	
	IBM-370	HP-1000
	Program	
	GRDYNMLT	PGT
User friendly	Moderately (one program to run)	Moderately (six programs to run in series; data input necessary for every program)
Documentation	Data input document, NASA CR-174747	No data input document
Input option	Good but complicated for higher level of input	Simple data file but no option for mass and damping
Output usage:		
Input table?	Yes	Yes
Tooth profile?	↓	No
Mesh load?	↓	Yes
Flash temperature?	↓	No
Hertz stress?	↓	No
Bending stress?	↓	No
Stiffness?	↓	Yes
Sun motion?	No	Yes

### Summary of Results

A dynamic analysis of a multimesh-gear helicopter transmission system, the Army UH-60A Black Hawk transmission, is presented. Three major categories of analysis were performed: a dynamic analysis using program GRDYNMLT, a parametric study with damping ratio variation and correlation with experimental data, and a comparison of the computer programs GRDYNMLT and PGT. Each category was examined under three phases of study: the dynamic characteristics of each gear mesh, harmonic excitation for multiple-tooth passes, and maximum mesh load with speed variations. The results of this study can be summarized as follows:

1. Computer programs GRDYNMLT and PGT both predict similar levels of dynamic mesh load for a three-planet-gear transmission.
2. The computer program GRDYNMLT has many options in both analytical and application capability, whereas PGT operates with only three planets, one load, and a floating sun option.
3. With the use of program FREPL, analytical results and experimental data can be compared in both the time and frequency domains. Good correlations have been obtained

through this comparison on the UH-60A Black Hawk transmission system.

4. The mesh damping ratios of the sun-planet and ring-planet meshes can be quite different in magnitude. A correlation with experimental data can provide a better estimate of the realistic damping ratios.

5. Because of nonsynchronous meshing of the planetary system, the UH-60A Black Hawk transmission system would cause considerable excitation in the multiple harmonics of the tooth-pass frequency. With the nonsynchronous phasing arrangement of the planetary gear, the fourth harmonic can be dominantly excited.

6. Tooth-spacing error can further amplify the asymmetric load distributions in the mesh. For light mesh damping ratios, several complete engagement-disengagement cycles can result

in a single-tooth pass between a pair of teeth. This can cause a higher peak mesh load even though the average mesh load is slightly lower.

7. A mesh load excited at a multiple harmonic tooth-pass frequency can be further amplified by tooth-profile modification with tip relief.

8. Tooth-profile modification can reduce the peak tooth-load amplitude at tooth engagement-disengagement even though the maximum peak load during the tooth pass has increased.

Lewis Research Center  
National Aeronautics and Space Administration  
Cleveland, Ohio, October 22, 1987

## Appendix A Explanation of Curves on Gear-Tooth Dynamics Figures

The distances along the line of action shown in figures 3, 6 to 10, 12, 13, 15, and 22 were normalized with respect to the circular pitch of the meshing gear. The existence of two load-versus-stress curves during the single-tooth pass indicated that the contact ratio was larger than unity (i.e., contact began on the second tooth while the first tooth was still in contact). The single-tooth pass period shown in the figures started when the first tooth in the first mesh arrived at pitch diameter. In figure 15, the phase shift due to the synchronous phasing can

be seen with reference to the phasing constants discussed in appendix B. Since a steady-state operating condition was assumed in this study, the dynamics on each tooth will be repeated for consecutive tooth passes. In other words, a complete description of the tooth dynamics can be obtained by continuing the first curve with the second curve (dashed line) for an extended period. The total length of this tooth in action in the normalized scale will be the mesh contact ratio.

## Appendix B Calculation of Planet-Mesh Phasing Constants

The normalized phasing constants shown in table II indicate the start of various planet-mesh engagements relative to a referenced single-tooth-pass period. For equally spaced planets, the sun-planet phasing constants are determined by assuming that the first planet mesh has a phasing constant of zero. The remaining sun-planet phasing constants for each planet  $K_{sp}$  are determined by

$$K_{sp} = (P_N - 1)F_{Rs}$$

where

- $P_N$  planet number
- $F_{Rs}$  fractional remainder of  $N_{st}/N_p$
- $N_{st}$  number of sun-gear teeth
- $N_p$  number of planets

The ring-planet phasing constants  $K_{rp}$  are determined similarly to those for the sun-planet. For planets with an odd number of teeth,

$$K_{rp} = (P_N - 1)F_{Rr}$$

where

- $F_{Rr}$  fractional remainder of  $N_{rt}/N_p$
- $N_{rt}$  number of ring-gear teeth
- For planets with an even number of teeth,

$$K_{rp} = K_{sp} + 0.5$$

The reason is that the ring gear is offset by 0.5 from the sun gear (180° out of phase).



## References

1. Terauchi, Y.; Nadano, H.; and Nohara, M.: On the Effect of the Tooth Profile Modification on the Dynamic Load and the Sound Level of the Spur Gear. *JSME Bull.*, vol. 25, no. 207, Sept. 1982, pp. 1474-1481.
2. Welbourn, D.B.: Gear Noise Spectra—A Rational Explanation. *ASME Paper 77-DET-38*, Sept. 1977.
3. Cornell, R.W.: Compliance and Stress Sensitivity of Spur Gear Teeth. *J. Mech. Des.*, vol. 103, no. 2, Apr. 1981, pp. 447-459.
4. Cornell, R.W.; and Westervelt, W.W.: Dynamic Tooth Loads and Stressing for High Contact Ratio Spur Gears. *J. Mech. Des.*, vol. 100, no. 1, Jan. 1978, pp. 69-76.
5. Pike, J.A.: Interactive Multiple Spur Gear Mesh Dynamic Load Program. *NASA CR-165514*, 1981.
6. Boyd, L.S.; and Pike, J.A.: Multimesh Gear Dynamics Program Evaluation and Enhancements. *NASA CR-174747*, 1985.
7. August, R., et al.: Dynamics of Planetary Gear Trains. *NASA CR-3793*, 1984.
8. Mitchell, A.M.; Oswald, F.B.; and Coe, H.H.: Testing of UH-60A Helicopter Transmission in NASA Lewis 2240-kW (3000-hp) Facility. *NASA TP-2626*, 1986.
9. Mancini, J.H.: An Overview of Advancements in Helicopter Transmission Design. *Advanced Power Transmission Technology*, NASA CP-2210, 1983, pp. 109-122. (Also AVRADCOM TR-82-C-16.)
10. Braddock, C.E.; and Battles, R.A.: Design of an Advanced 500-hp Helicopter Transmission. *Advanced Power Transmission Technology*, NASA CP-2210, 1983, pp. 123-140. (Also AVRADCOM TR-82-C-16.)
11. Choy, F.K.; Townsend, D.P.; and Oswald, F.B.; Experimental and Analytical Evaluation of Dynamic Load and Vibration of a 2240-kW (3000-hp) Rotorcraft Transmission. *NASA TM-88975*, 1987.
12. Dudley, D.W.: *Handbook of Practical Gear Design*. McGraw-Hill, 1984.
13. Coy, J.J.; Townsend, D.P.; and Zaretsky, E.W.: Dynamic Capacity and Surface Fatigue Life for Spur and Helical Gears. *J. Lubr. Technol.*, vol. 98, no. 2, Apr. 1976, pp. 267-276.
14. Otnes, R.K.; and Enochson, L.D.: *Applied Time Series Analysis*, Vol. 1, Basic Techniques, Wiley-Interscience, 1978.
15. Drago, R.J.: An Improvement in the Conventional Analysis of Gear Tooth Bending Fatigue Strength. *AGMA P229.24*, American Gear Manufacturers Association, 1982.

ORIGINAL PAGE IS  
OF POOR QUALITY

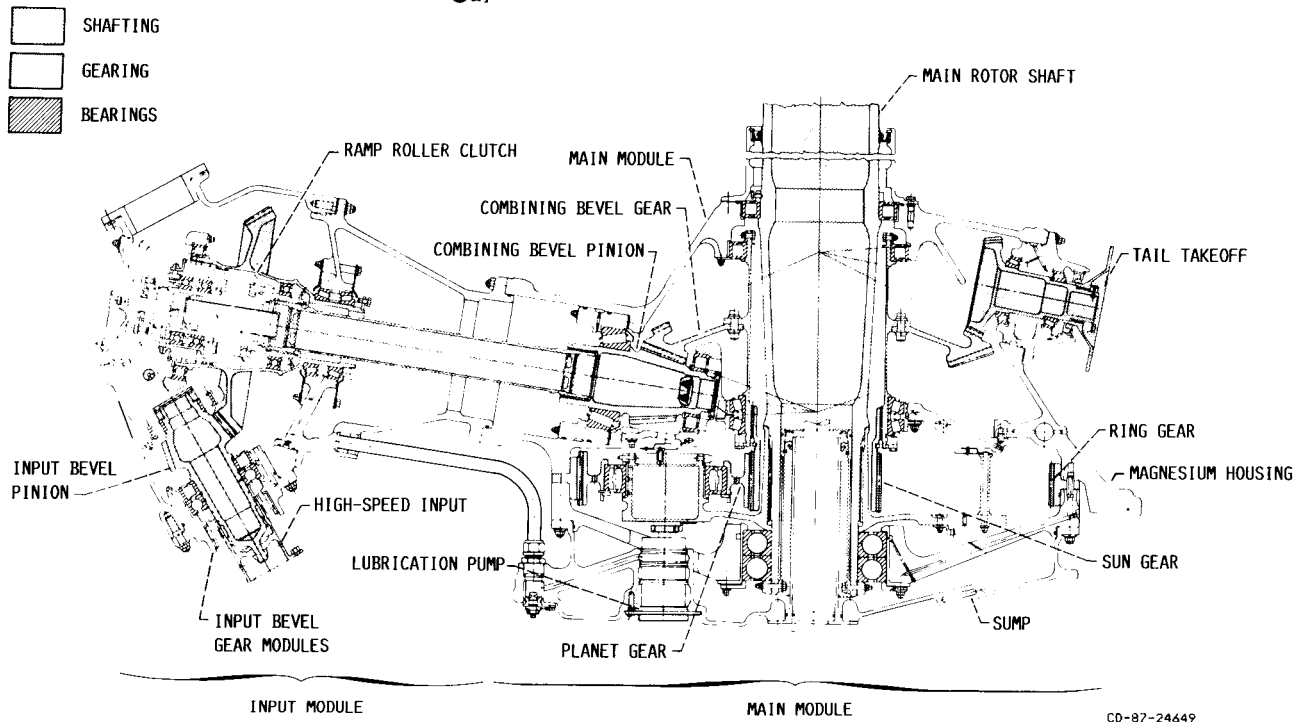


Figure 1.—Cross section of input module and tail of UH-60A helicopter transmission.

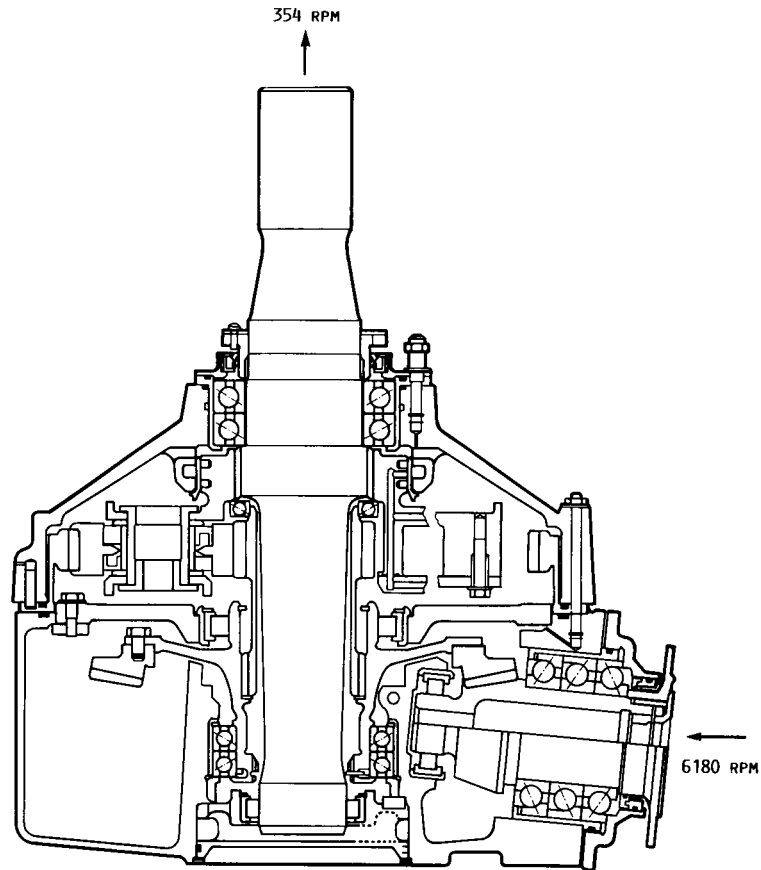
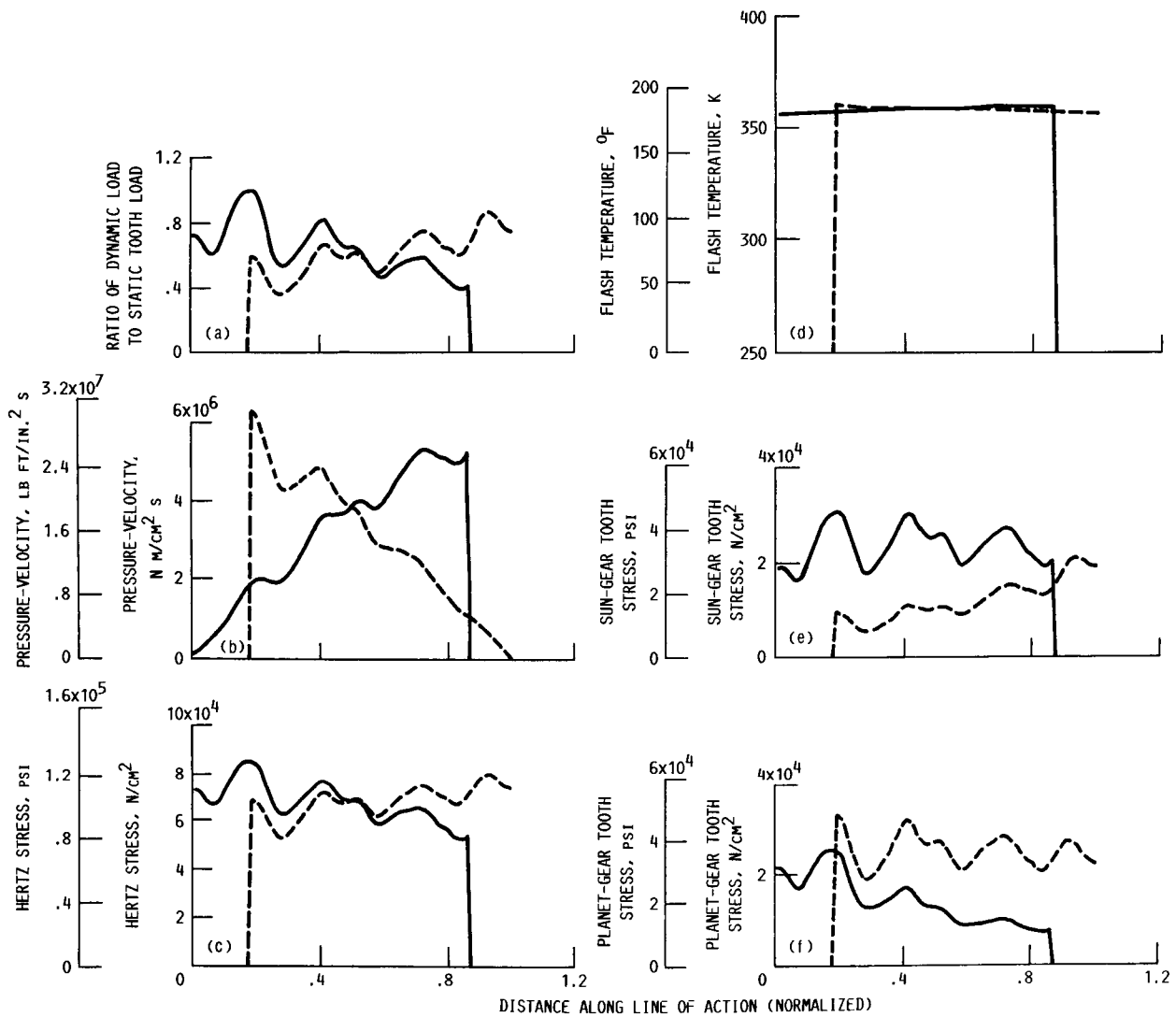
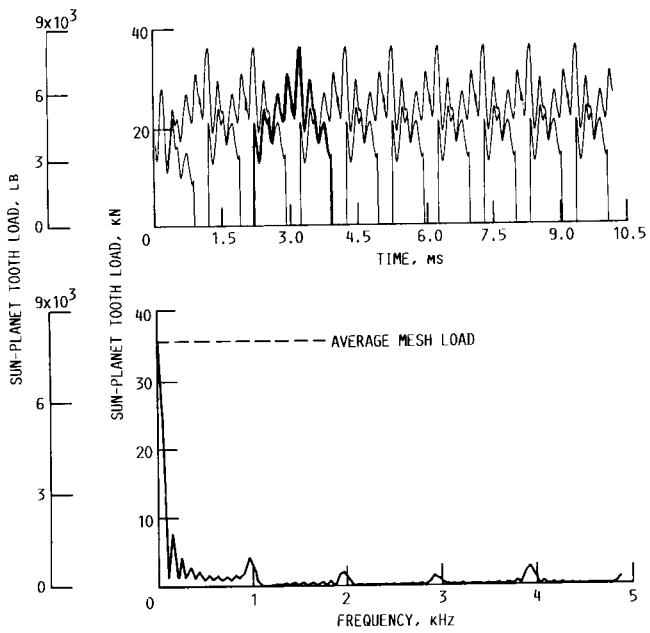


Figure 2.—NASA/Bell Helicopter 370-kW (500-hp) main rotor gearbox.



(a) Ratio of dynamic load to static tooth load. (d) Flash temperature.  
 (b) Pressure-velocity. (e) Sun-gear tooth stress.  
 (c) Hertz stress. (f) Planet-gear tooth stress.

Figure 3.—Dynamic output of first sun-planet gear mesh.



(a) As function of time.  
(b) As function of frequency.

Figure 4.—Gear load of first sun-planet mesh with spacing error.

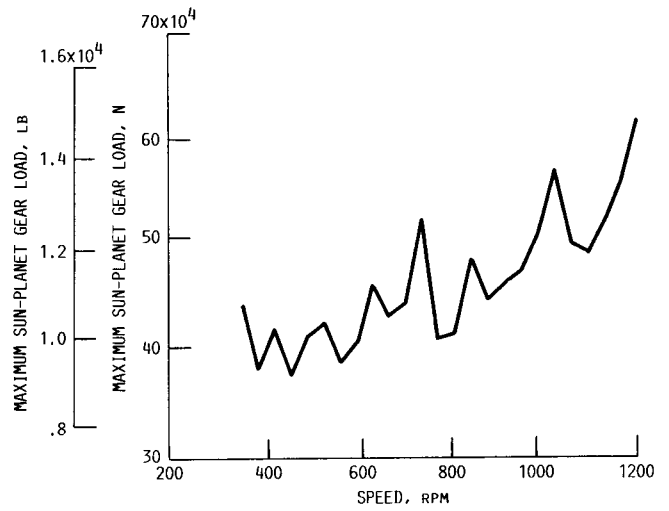


Figure 5.—Maximum gear load at first sun-planet mesh.

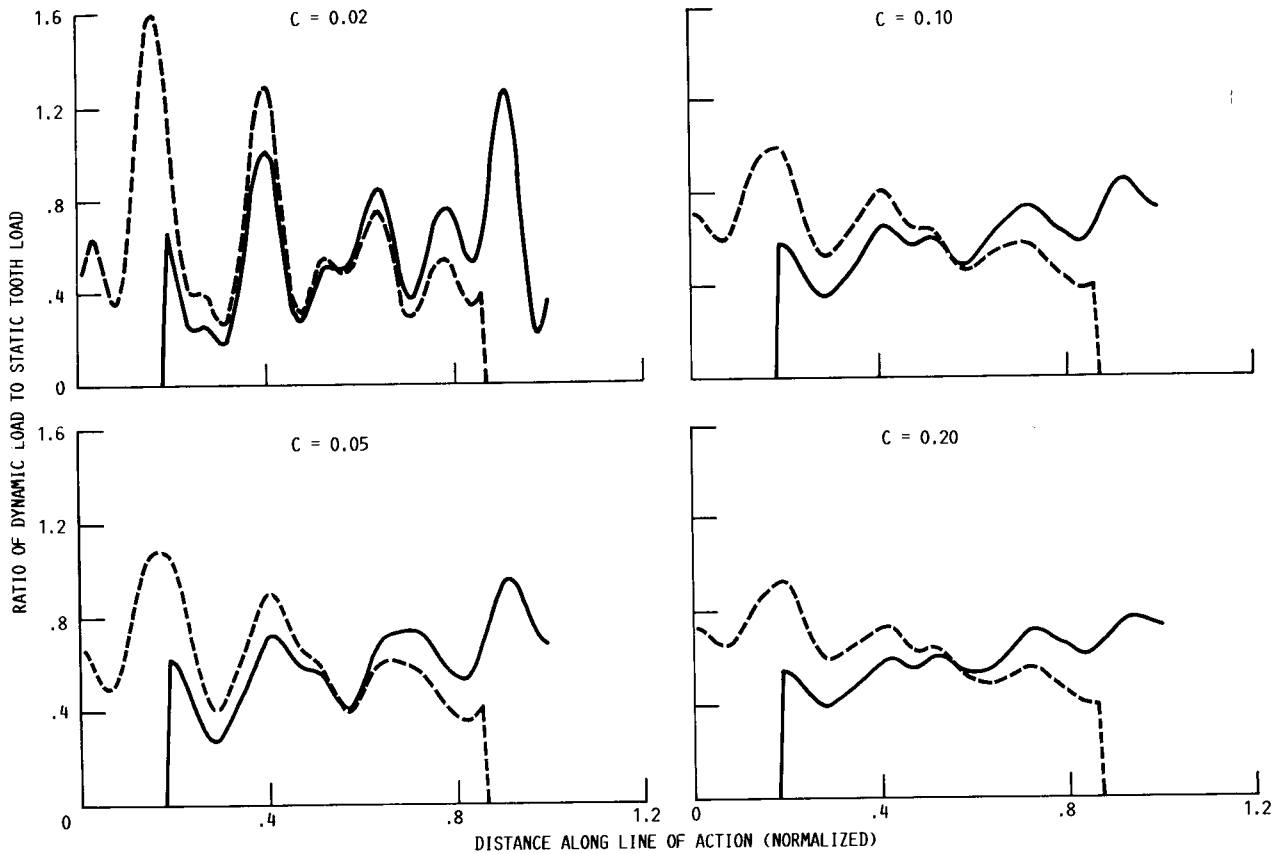


Figure 6.—Effects of mesh damping ratio  $c$  on sun-planet load. Sun-gear speed, 1206 rpm; input torque on sun gear, 15 000 N m (11 000 lb ft).

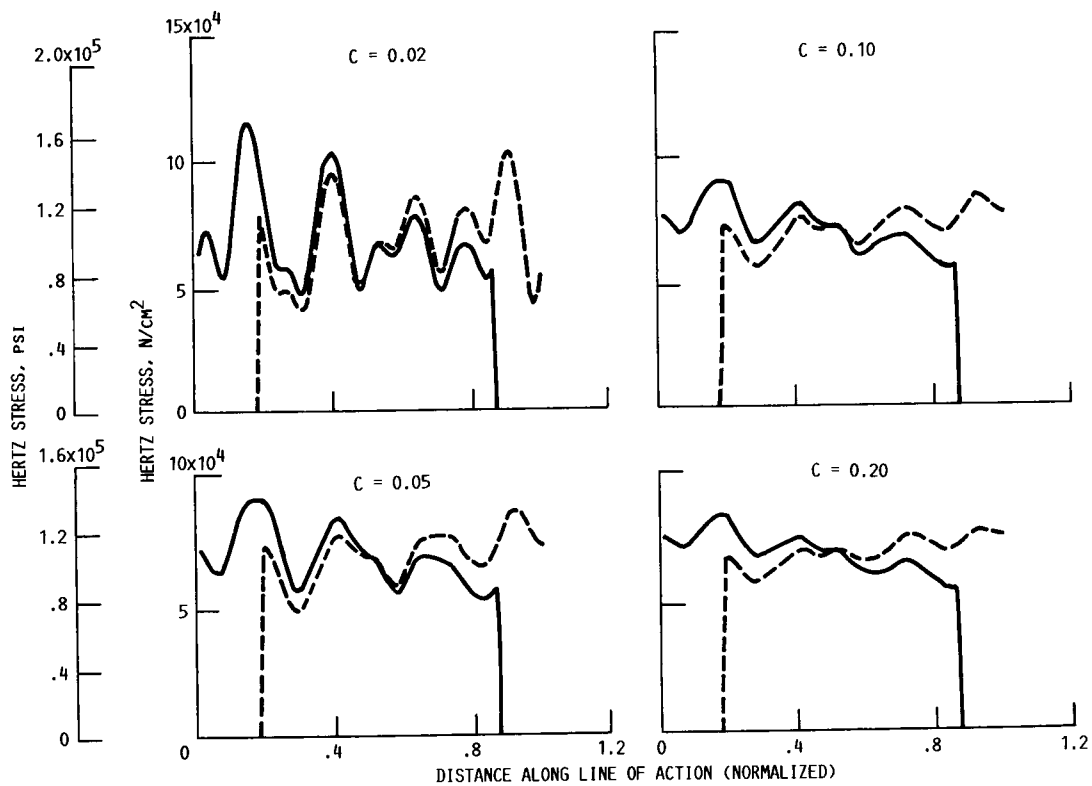


Figure 7.—Effects of mesh damping ratio  $c$  on sun-planet mesh Hertz stress.

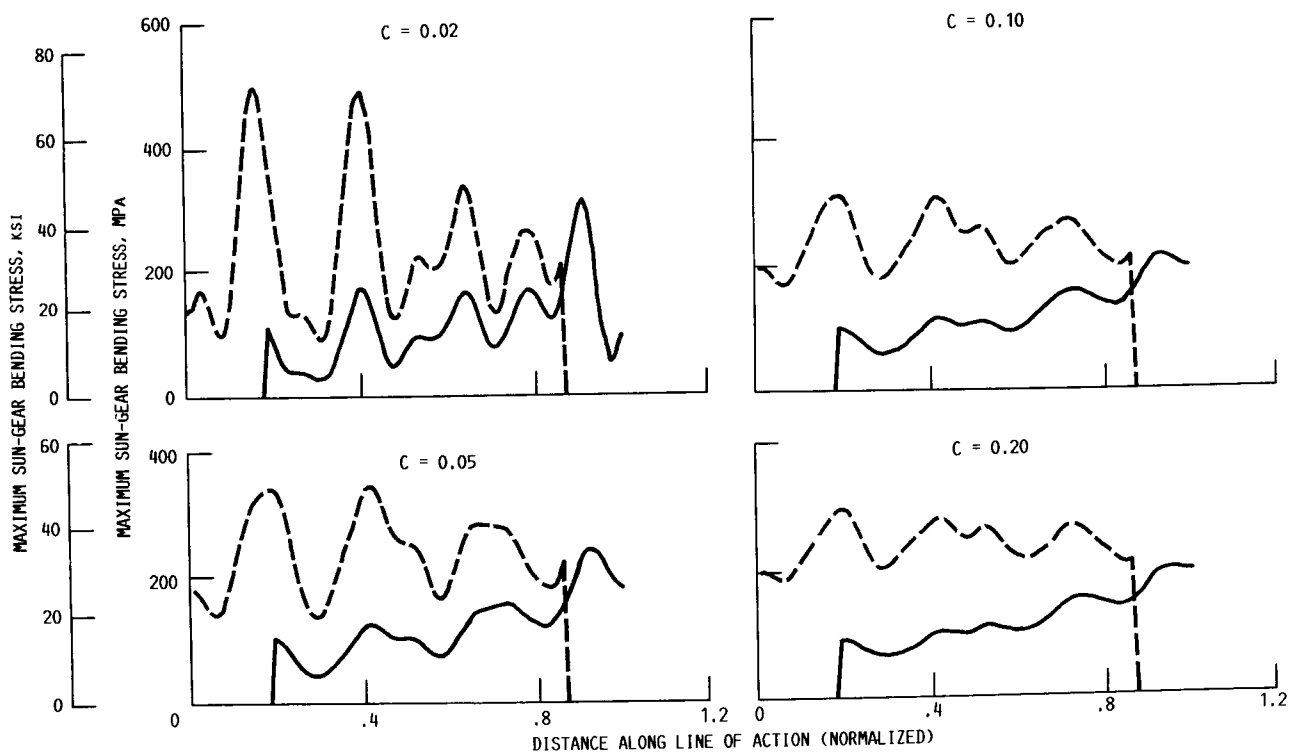


Figure 8.—Effects of mesh damping ratio  $c$  on sun-planet tooth-bending stress. Sun-gear speed, 1206 rpm; input torque on sun gear, 15 000 N m (11 000 lb ft).

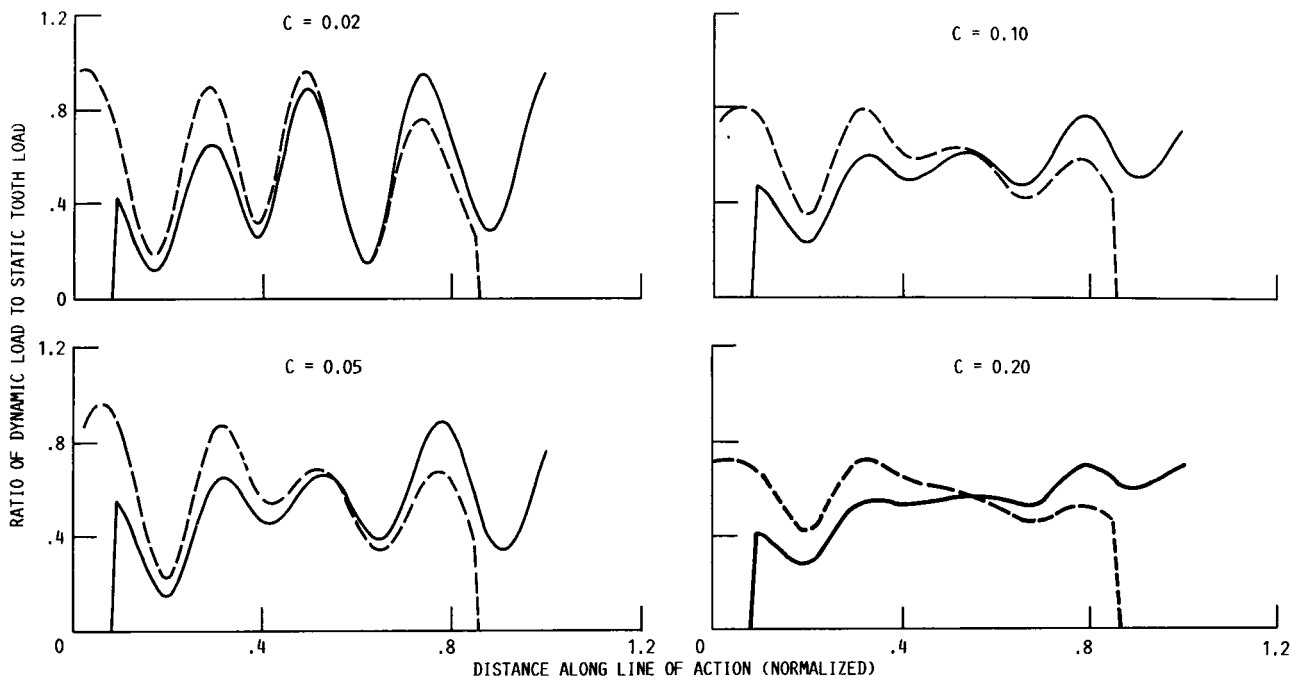


Figure 9.—Effects of mesh damping ratio  $c$  on ring-planet load. Sun-gear speed, 1206 rpm; input torque on sun gear, 15 000 N m (11 000 lb ft).

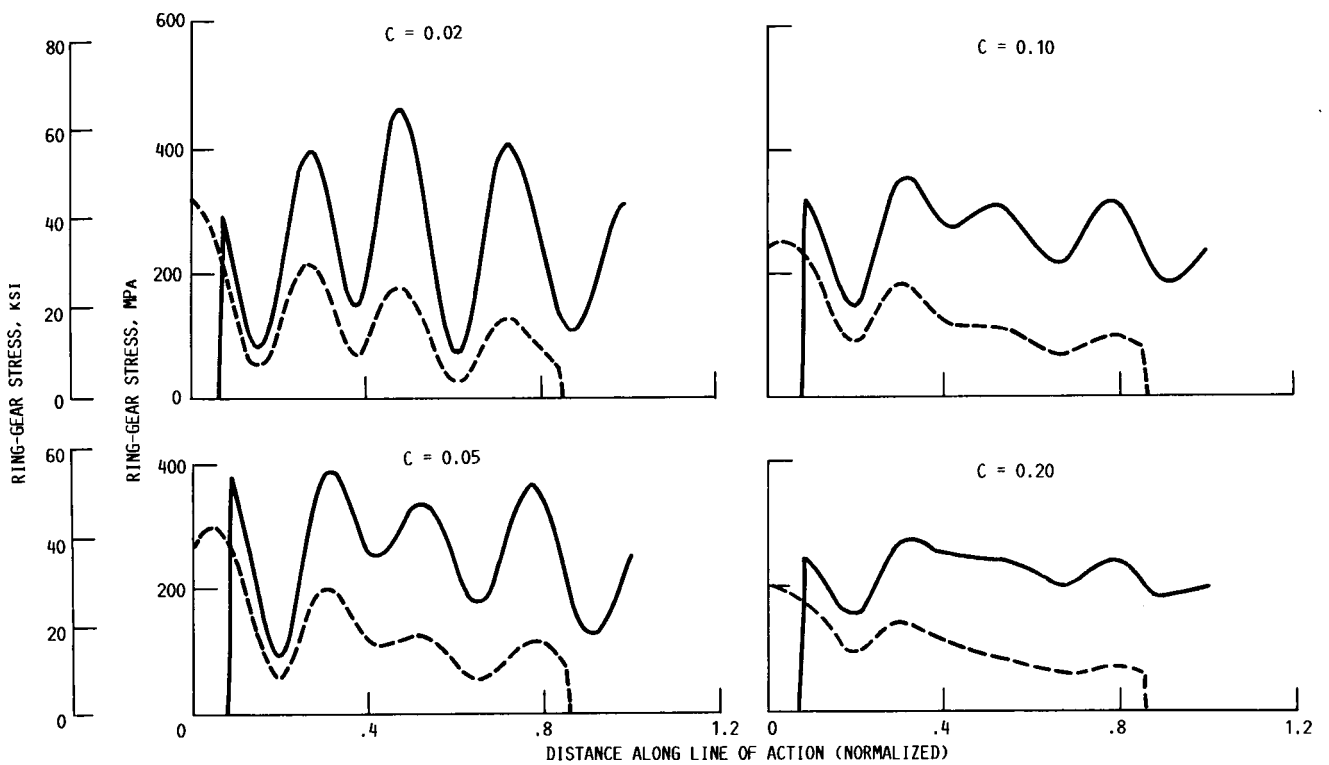


Figure 10.—Effects of mesh damping ratio  $c$  on ring-planet tooth-bending stress. Sun-gear speed, 1206 rpm; input torque on sun gear, 15 000 N m (11 000 lb ft).

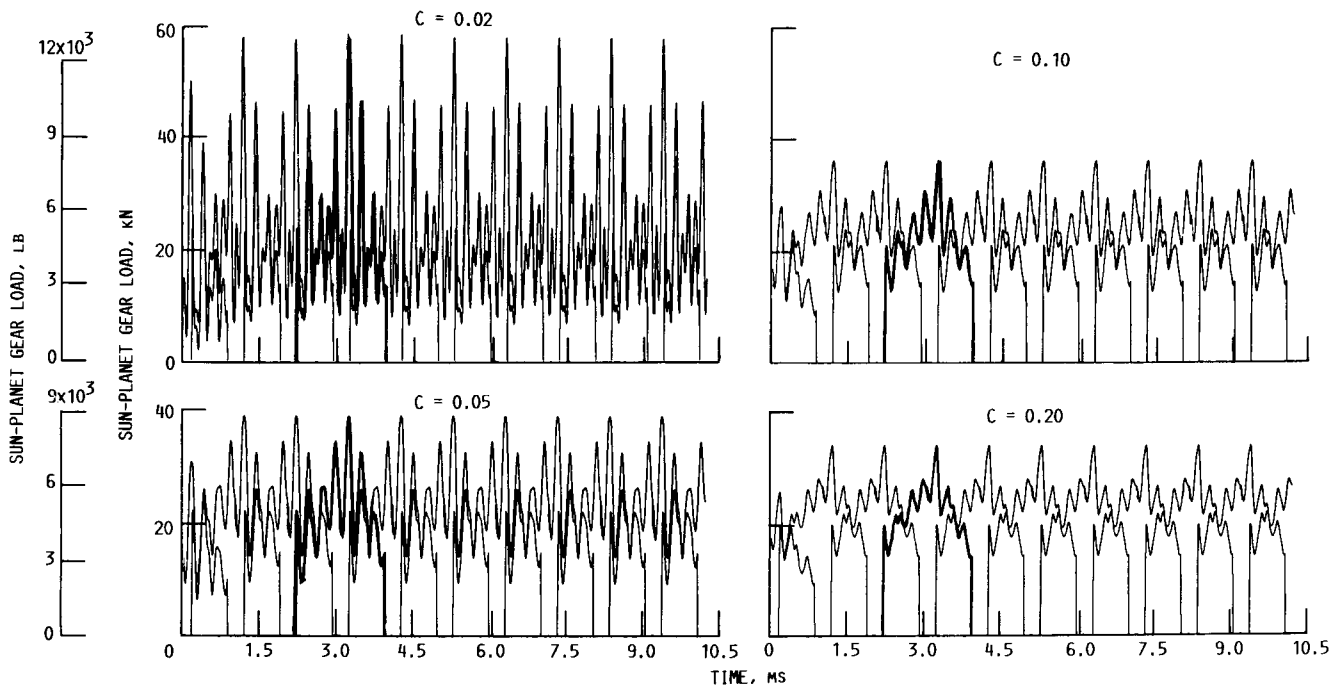


Figure 11.—Effects of mesh damping ratio  $c$  on sun-planet load with tooth-spacing error. Sun-gear speed, 1206 rpm; input torque on sun gear, 15 000 N m (11 000 lb ft).

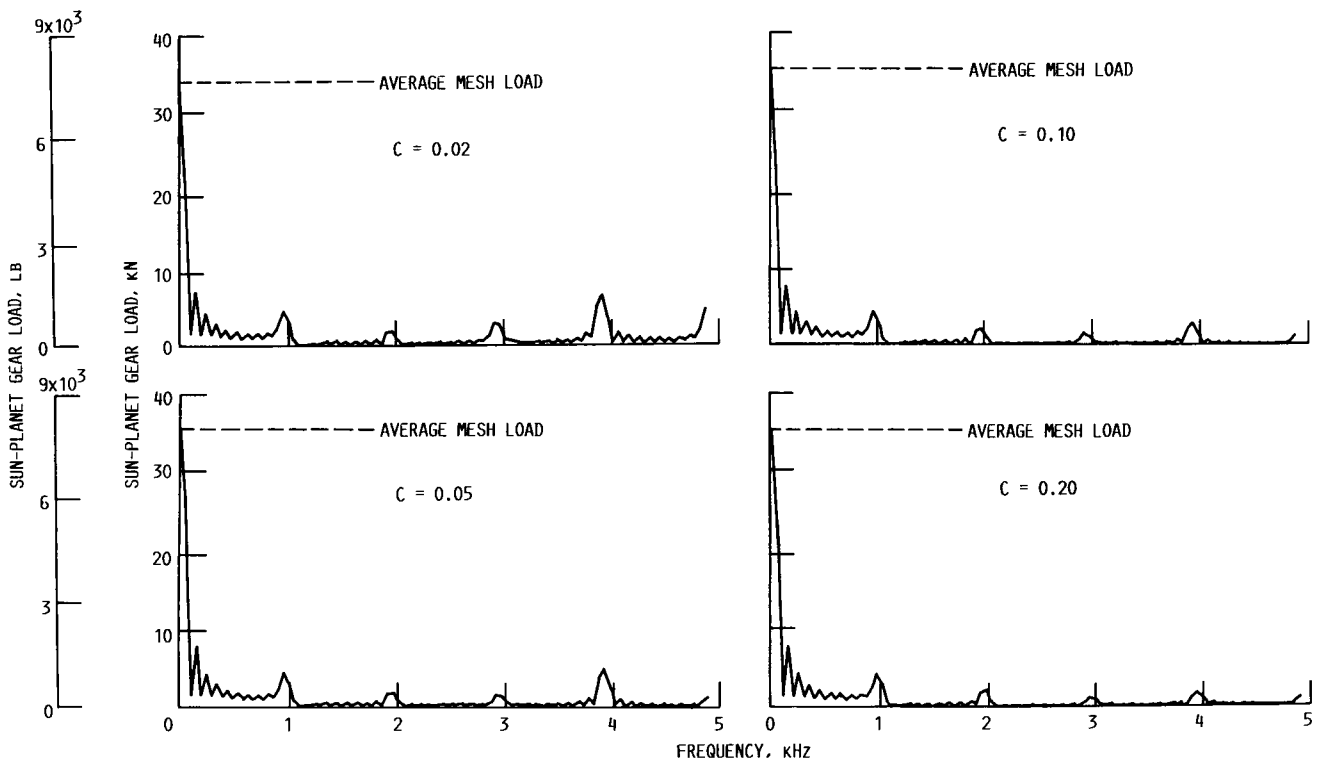


Figure 12.—Frequency-domain analysis of sun-planet load with effects of mesh damping ratio  $c$ . Sun-gear speed, 1206 rpm; input torque on sun gear, 15 000 N m (11 000 lb ft).

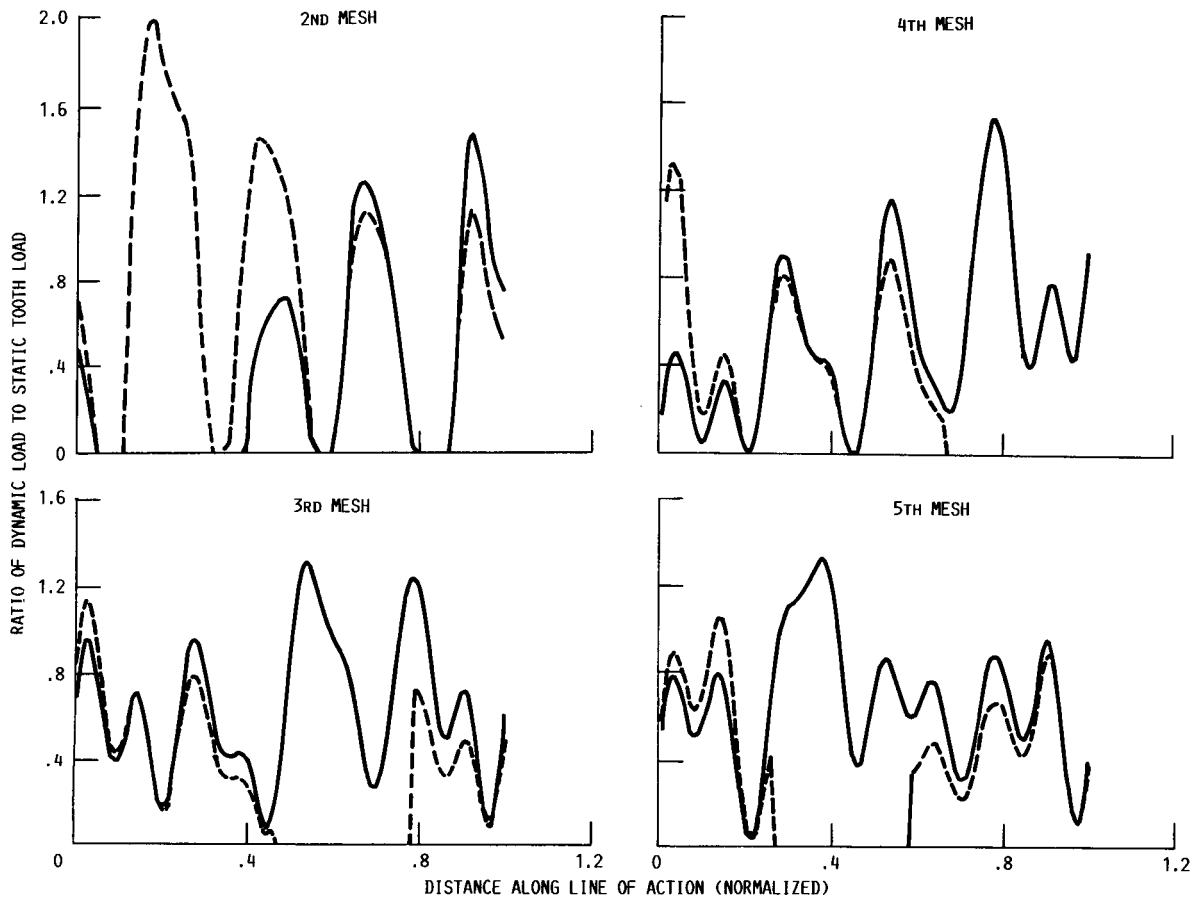


Figure 13.—Effect of planet location on sun-planet load with light damping. Mesh damping ratio,  $c$ , 0.02; sun-gear speed, 1206 rpm; input torque on sun gear, 15 000 N m (11 000 lb ft).

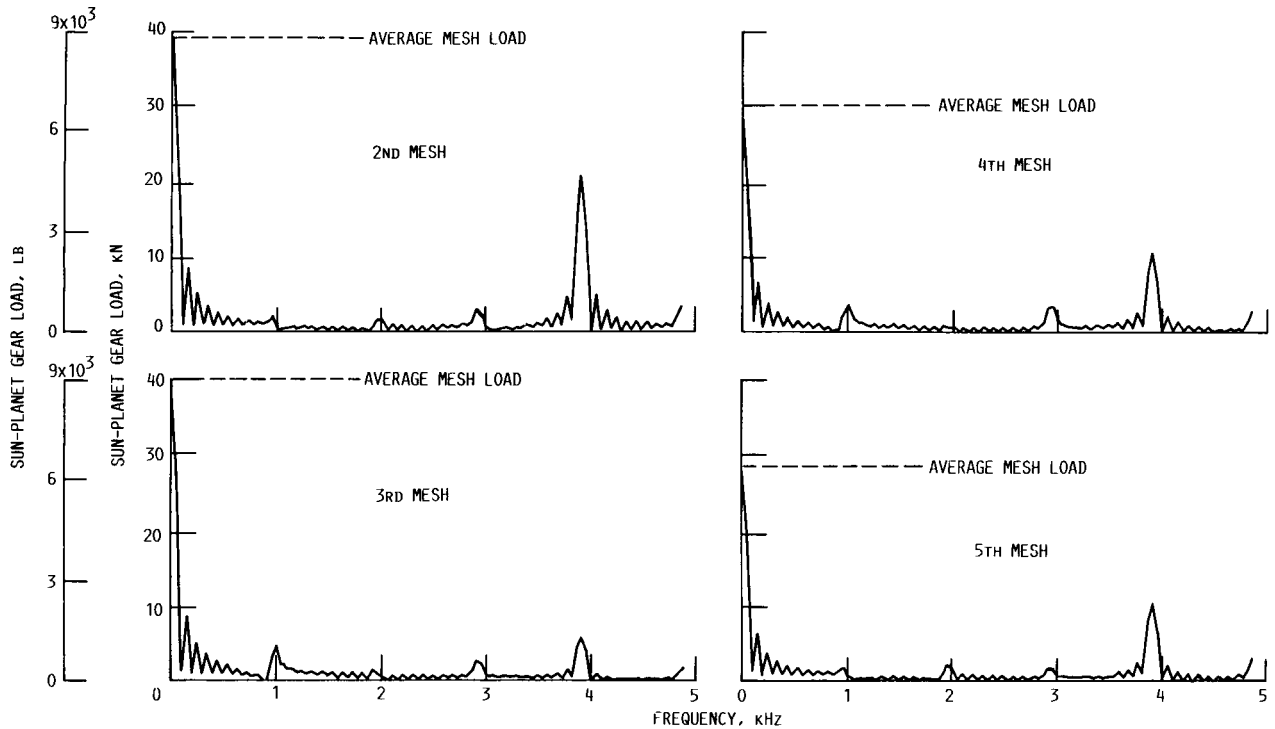


Figure 14.—Frequency components of sun-planet load with light damping. Mesh damping ratio,  $c$ , 0.02; sun-gear speed, 1206 rpm; input torque on sun gear, 15 000 N m (11 000 lb ft).



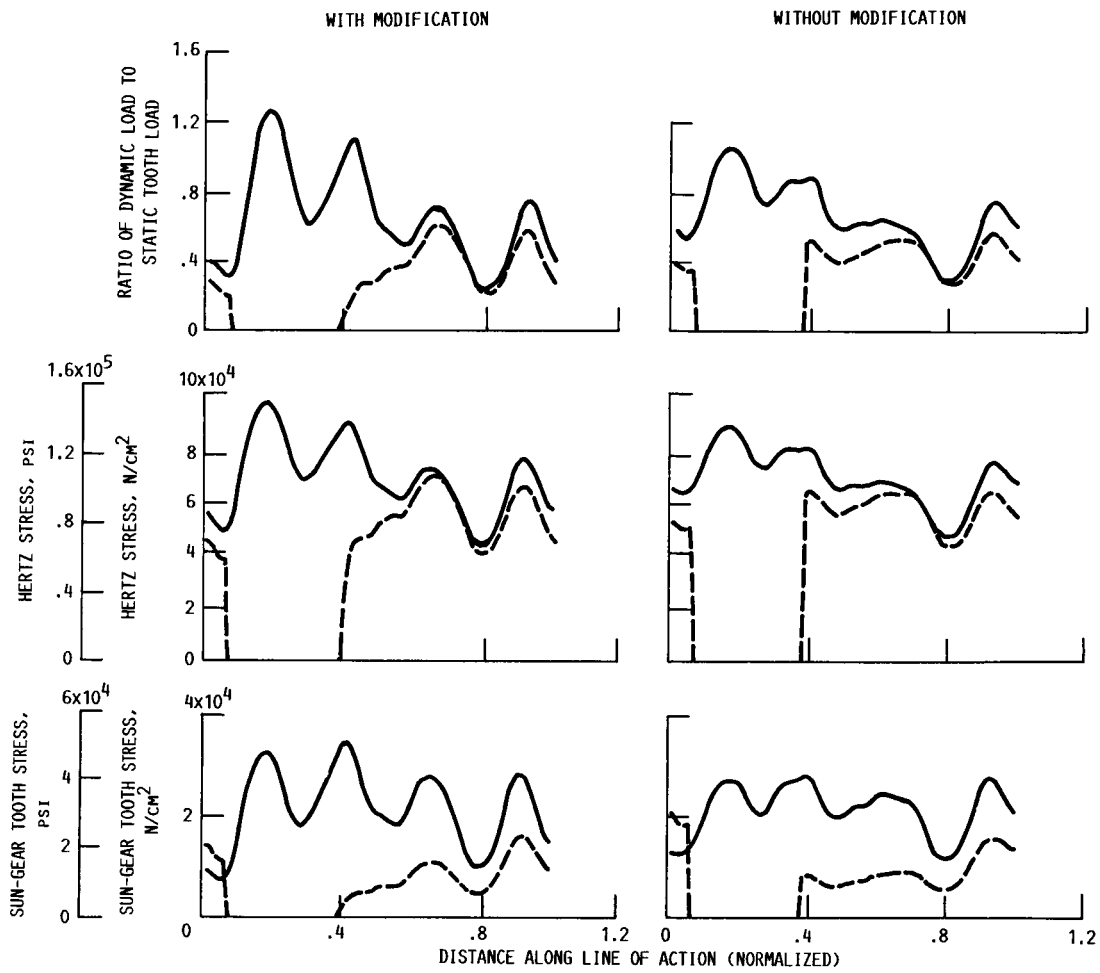
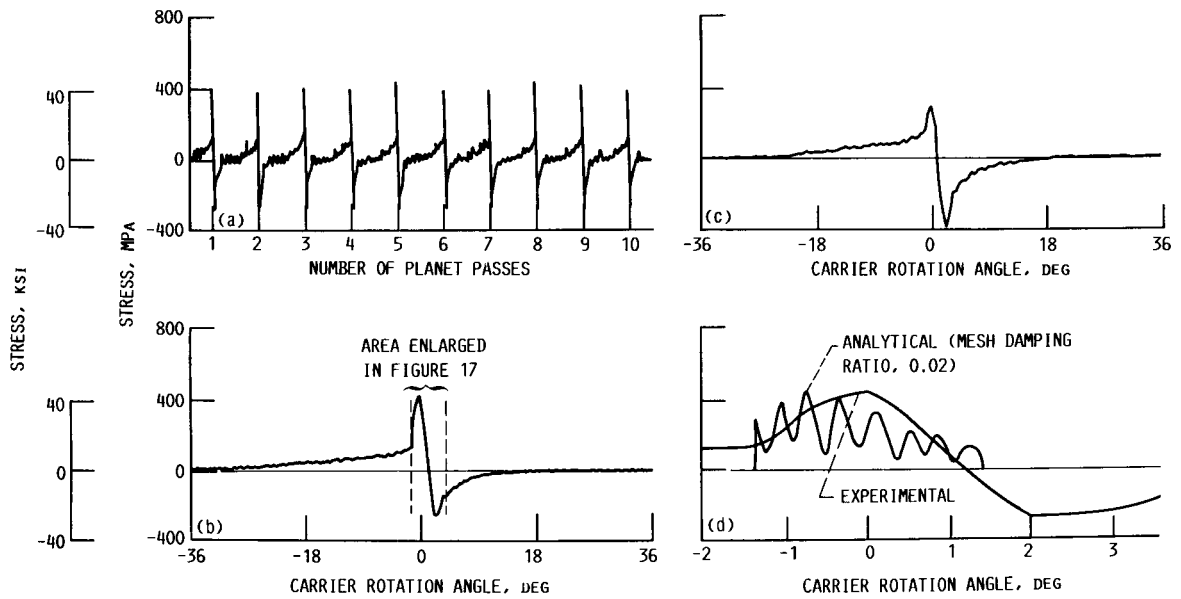
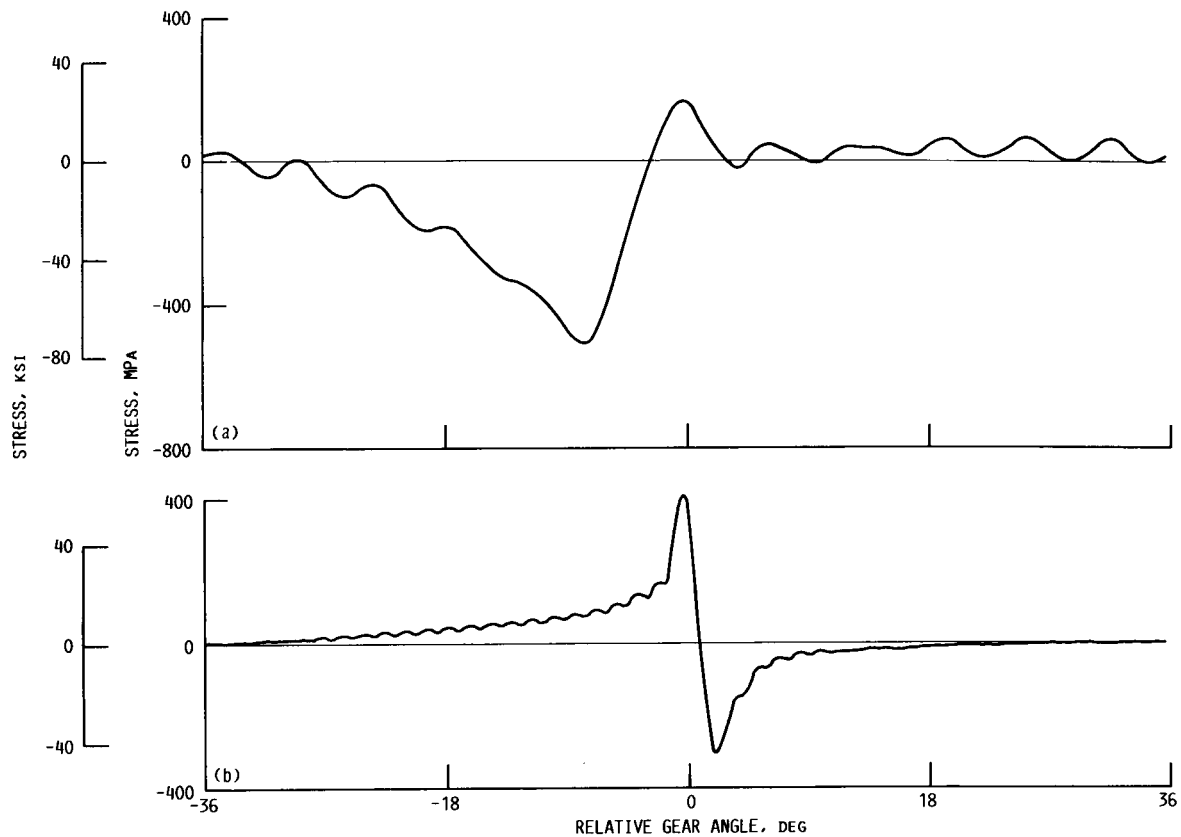


Figure 15.—Effects of tooth-profile modification with tip relief.



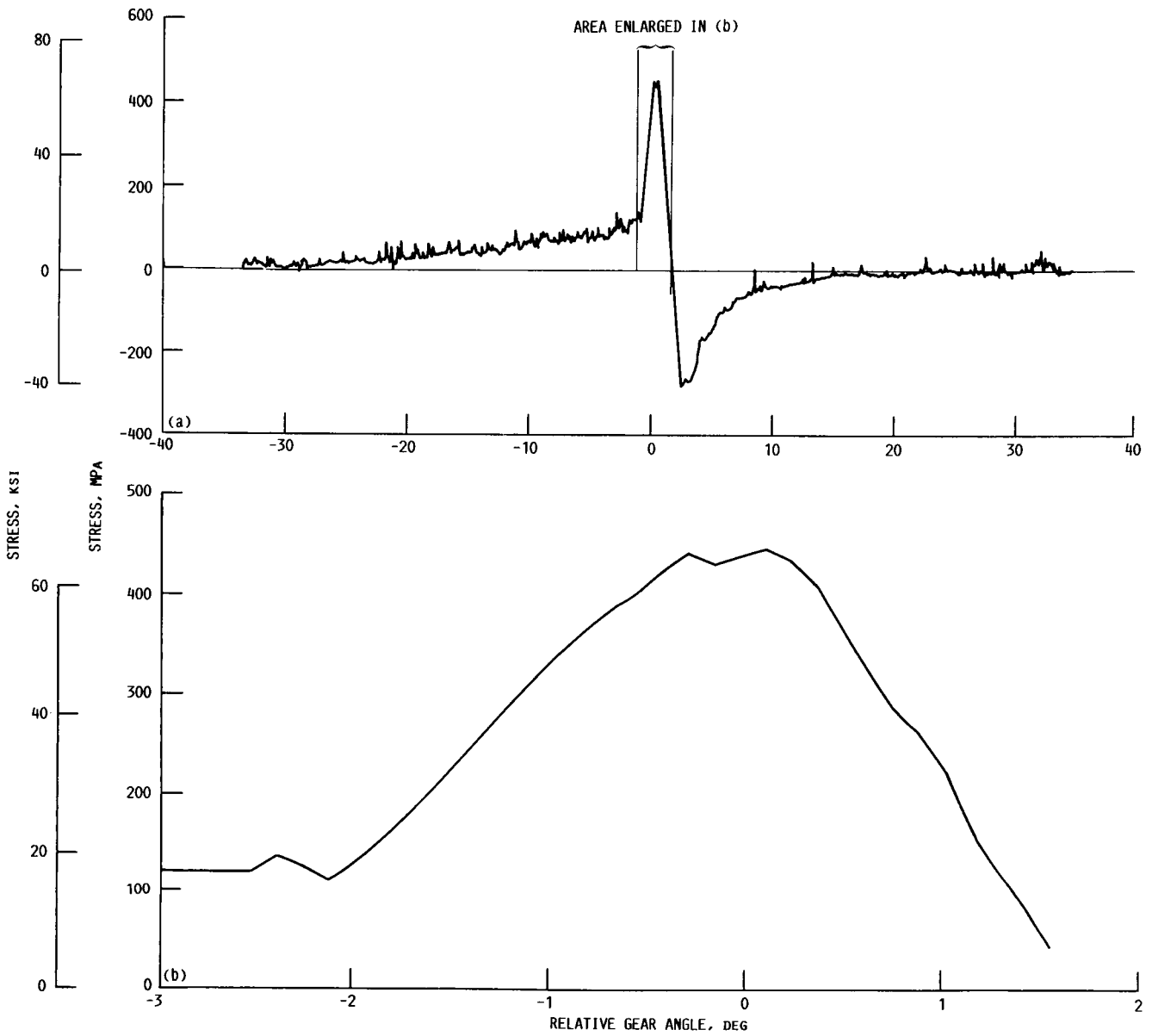
(a) Fillet gages (showing 10 planet passes).  
 (b) Fillet gage cycle (averaged from 10 planet passes).  
 (c) Root gage cycle (averaged from 10 planet passes).  
 (d) Comparison of analytical and experimental results for one tooth mesh.

Figure 16.—Stress in ring gear.



(a) Root stress on sun gear. Maximum stress, 162 MPa; minimum stress, 516 MPa; maximum predicted stress, 495 MPa; mesh damping ratio, 0.02.  
 (b) Fillet stress on ring gear. Maximum stress, 409 MPa; minimum stress 310 MPa; maximum predicted stress, 295 MPa; mesh damping ratio, 0.10.

Figure 17.—Experimental data on bending stresses with averages of 10 data points. Sun-gear speed, 1206 rpm; input torque on sun gear, 15 000 N m (11 000 lb ft).



(a) Single trace data on ring-gear bending stress without filter.

(b) Zoom-in data on maximum peak of figure 18(a).

Figure 18.—Single trace data on ring-gear bending stress without filter. Sun-gear speed, 1206 rpm; input torque on sun gear, 15 000 N m (11 000 lb ft).

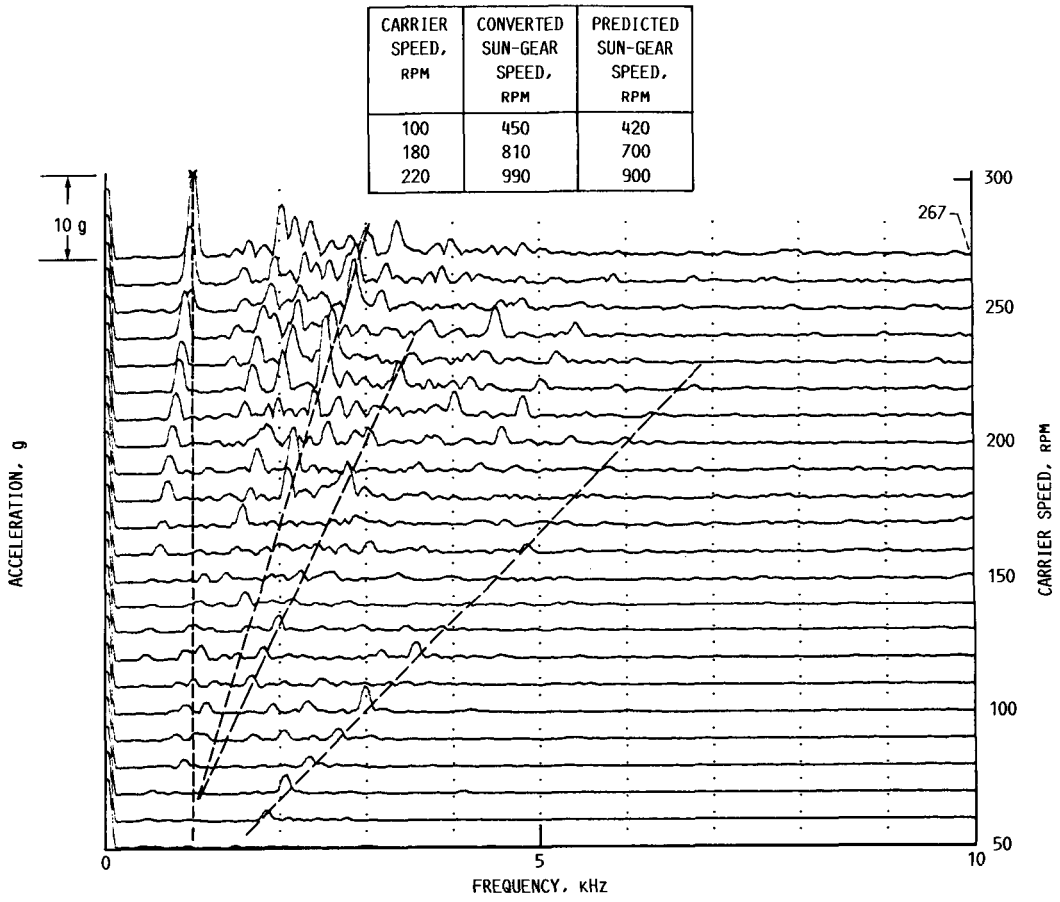


Figure 19.—Experimental vibration data at several speeds with vibration accelerometer located near ring gear. Input torque on sun gear, 5000 N m (3700 lb ft).

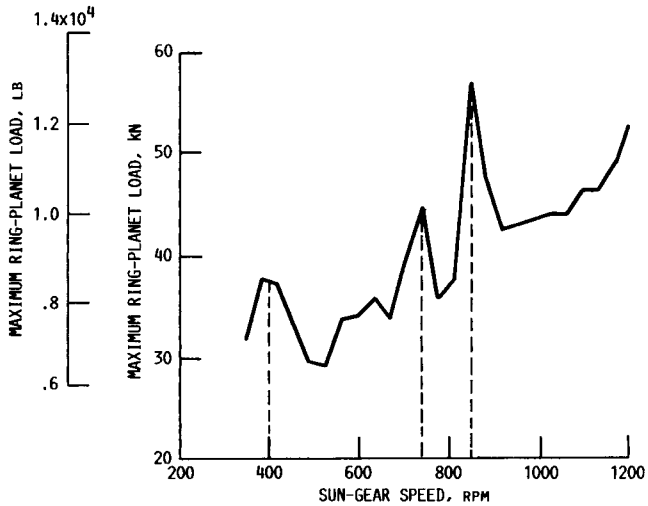


Figure 20.—Maximum ring-gear bending stress with speed variation.

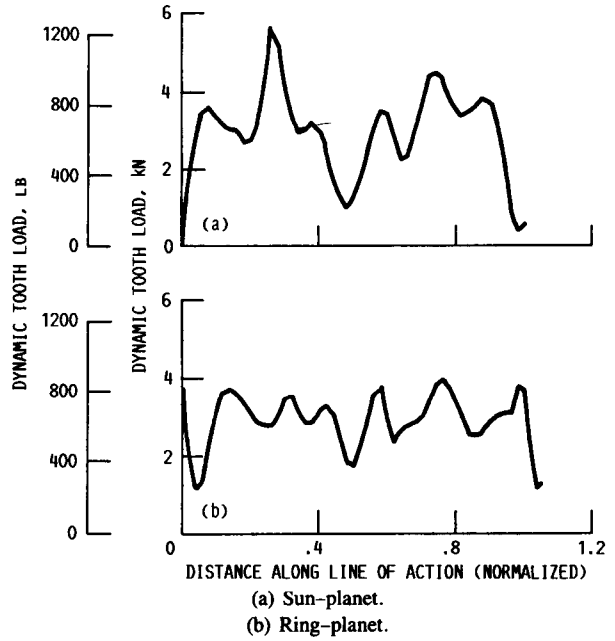


Figure 21.—Dynamic gear-tooth load from PGT for one tooth-mesh cycle. Speed, 1200 rpm; input torque, 510 N m (375 lb ft).

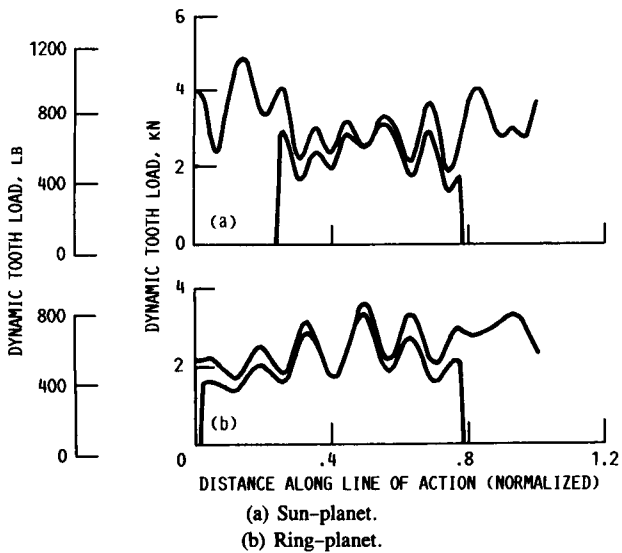


Figure 22.—Dynamic gear-tooth load from GRDYNMLT for one tooth-mesh cycle. Speed, 1200 rpm; input torque, 510 N m (375 lb ft).

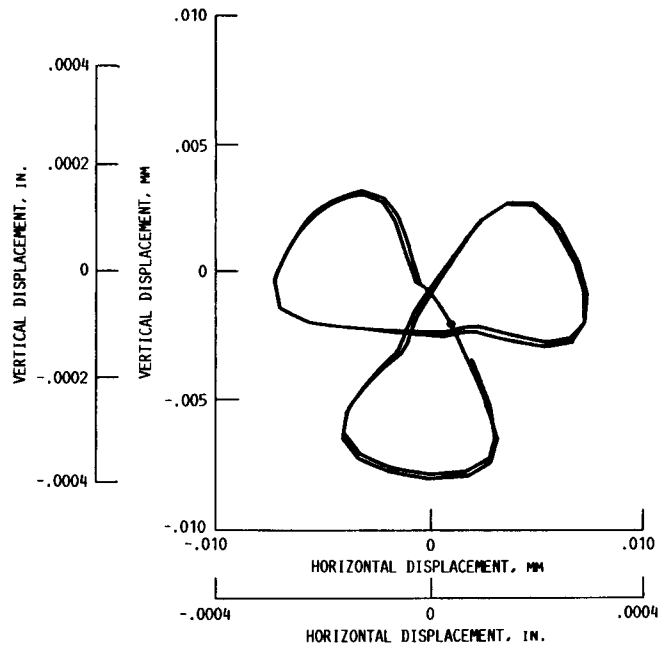


Figure 23.—Orbit of three-planet-system sun gear from PGT.



# Report Documentation Page

1. Report No. NASA TP-2789		2. Government Accession No.		3. Recipient's Catalog No.	
4. Title and Subtitle Dynamic Analysis of Multimesh-Gear Helicopter Transmissions			5. Report Date February 1988		
			6. Performing Organization Code		
7. Author(s) Fred K. Choy, Dennis P. Townsend, and Fred B. Oswald			8. Performing Organization Report No. E-3191		
			10. Work Unit No. 505-62-51		
9. Performing Organization Name and Address National Aeronautics and Space Administration Lewis Research Center Cleveland, Ohio 44135-3191			11. Contract or Grant No.		
			13. Type of Report and Period Covered Technical Paper		
12. Sponsoring Agency Name and Address National Aeronautics and Space Administration Washington, D.C. 20546-0001			14. Sponsoring Agency Code		
			15. Supplementary Notes		
16. Abstract <p>A dynamic analysis of multimesh-gear helicopter transmission systems was performed by correlating analytical simulations with experimental investigations. The two computer programs used in this study, GRDYNMLT and PGT, were developed under NASA/Army sponsorship. Parametric studies of the numerical model with variations in mesh damping ratios, operating speeds, tip-relief tooth modifications, and tooth-spacing errors were performed to investigate the accuracy, application, and limitations of the two computer programs. Although similar levels of dynamic loading were predicted by both programs, the computer code GRDYNMLT was found to be superior and broader in scope. Results from analytical work were also compared with experimental data obtained from the U.S. Army's UH-60A Black Hawk 2240-kW (3000-hp) class, twin-engine helicopter transmission tested at the NASA Lewis Research Center. Good correlation in gear stresses was obtained between the analytical model simulated by GRDYNMLT and the experimental measurements. More realistic mesh damping can be predicted through experimental data correlation.</p>					
17. Key Words (Suggested by Author(s)) Gearing; Dynamic analysis; Multimesh; Gear dynamics; Gear vibrations; Transmissions			18. Distribution Statement Unclassified - Unlimited Subject Category 37		
19. Security Classif. (of this report) Unclassified		20. Security Classif. (of this page) Unclassified		21. No of pages 21	22. Price* A02